OPEN

Spectral Photon-Counting Detector CT for Comprehensive Evaluation of Carotid Plaque and Stenosis

Juul Bierens, MSc, Jelske Kuijpers, BSc, Florentina M.E. Pinckaers, MD, PhD, Luca Saba, MD, PhD, Luc J.M. Smits, PhD, Robert J. van Oostenbrugge, MD, PhD, Thomas Flohr, PhD, M. Eline Kooi, PhD, and Alida A. Postma, MD, PhD

Background Conventional energy-integrating detector (EID) CT is limited in differentiating soft-plaque components due to overlapping attenuation values and is frequently affected by calcification-related blooming artifacts that obscure the vessel lumen and may overestimate stenosis. Photon-counting detector CT (PCD-CT) can provide enhanced spatial resolution and spectral discrimination compared with conventional EID-CT, potentially improving carotid plaque characterization and mitigating artifact-related limitations. This study systematically evaluated image quality, plaque component attenuation, and stenosis visualization across spectral PCD-CT reconstructions.

Methods We retrospectively included patients who underwent PCD-CT for carotid stenosis assessment. Four monoenergetic (ME 40, 55, 70, and 85 keV), PureLumen (PL), and virtual noncontrast (VNC) reconstructions were analyzed. Signal-to-noise ratio (SNR), contrast-to-noise ratio (CNR), edge sharpness, plaque area, degree of NASCET stenosis, and attenuation of plaque components (intraplaque hemorrhage, lipid-rich necrotic core, fibrotic tissue, calcification) were compared using repeated-measures ANOVA with Bonferroni correction.

Results Our study included 27 patients (16 men, age: 74.5 ± 9.1 y) with 50 plaques. CNR, SNR, and noise decreased with increasing ME levels ($P < 0.001$). PL yielded CNR and sharpness comparable to ME55, whereas VNC exhibited a near-zero lumen signal. Stenosis remained consistent across ME reconstructions (44% to 45%, $P = 1.00$), but significantly reduced for PL (38%, $P < 0.001$). Lower-energy reconstructions (ME40/ME55) improved the separation of attenuation values between the lumen and the various plaque components.

Conclusion Low-energy PCD-CT reconstructions enhance CNR and sharpness while maintaining consistent plaque and stenosis measurements. The PL algorithm may improve the assessment of calcified plaques, where conventional reconstructions may overestimate stenosis. PCD-CT shows promise for advanced plaque composition evaluation, but further validation against MRI and histology is warranted.

Key Words: carotid plaque, photon-counting detector, computed tomography angiography, stenosis, atherosclerosis

(*Invest Radiol* 2026;00:000–000)

Carotid atherosclerosis accounts for ~10% to 20% of ischemic strokes.[1] Its true contribution is likely higher, as stroke in a patient with nonstenotic carotid plaque is classified as cryptogenic.[2] Rupture of a vulnerable atherosclerotic plaque can trigger thrombosis and ultimately lead to cerebral ischemia.[3] Plaque vulnerability is largely determined by composition, and several features are associated with an increased risk, including a large lipid-rich necrotic core (LRNC) and intraplaque hemorrhage (IPH).[4] While clinical decision-making still primarily relies on stenosis degree, there is a growing shift toward incorporating plaque composition, underscoring the need for advanced imaging techniques capable of identifying these features.[5,6]

Computed tomography angiography (CTA) is widely used to evaluate plaque presence and the degree of stenosis in clinical practice. However, reliable characterization of soft-plaque components, such as LRNC and IPH, is currently only feasible with magnetic resonance imaging (MRI).[7,8] Identifying these components with a conventional energy-integrating detector (EID)-CT is challenging due to overlapping HU values.[9] In addition, calcified plaques on CT frequently produce blooming artifacts that exaggerate these high-density structures, obscure the true lumen, and can lead to overestimation of stenosis severity.[10]

Photon-counting detector CT (PCD-CT) may overcome some of these limitations. Unlike conventional EID-CT, which converts x-ray photons into light before generating electrical signals, photon-counting detectors directly convert each photon into an electrical signal.[11] Conventional detectors require septa that reduce spatial resolution, and these detectors sum photon energies into a single signal, thereby losing energy-specific information. Photon-counting detectors directly convert each photon into an electrical signal, which enables discrimination of photon energies, allowing for spectral image reconstruction. By eliminating septa, PCD-CT improves spatial resolution.[12] Consequently, PCD-CT can provide reconstructions of virtual monoenergetic (ME), PureLumen (PL), and virtual noncontrast (VNC) images. ME reconstructions visualize photon attenuation at defined energy levels; VNC suppresses the iodine signal to simulate a noncontrast scan, and PL reconstructions remove

Received for publication February 5, 2026; and accepted for publication, after revision, March 19, 2026.

From the Department of Radiology and Nuclear Medicine, Maastricht University Medical Center, Maastricht, The Netherlands (J.B., J.K., F. M.E.P., T.F., M.E.K., A.A.P.); CARIM Cardiovascular Research Institute Maastricht, Maastricht University, Maastricht, The Netherlands (J.B., F.M.E.P., R.J.V.O., M.E.K.); Department of Radiology, University of Cagliari, Cagliari, Italy (L.S.); Department of Epidemiology, Maastricht University, Maastricht, The Netherlands (L.J.M.S.); Department of Neurology, Maastricht University Medical Center, Maastricht, The Netherlands (R.J.V.O.); MHeNS Mental Health and Neuroscience Research Institute Maastricht, Maastricht University, Maastricht, The Netherlands (A.A.P.).

The data sets generated during and/or analyzed during the current study are available from the corresponding author upon reasonable request.

Conflicts of interest and sources of funding: none declared.

Correspondence to: Alida A. Postma, MD, PhD, Department of Radiology and Nuclear Medicine, Maastricht University Medical Center, P.O. Box 5800, Maastricht 6202 AZ, The Netherlands. E-mail: l.jacobi@mumc.nl.

Supplemental Digital Content is available for this article. Direct URL citations are provided in the HTML and PDF versions of this article on the journal's website, www.investigativeradiology.com.

ISSN: 1536-0210
DOI: 10.1097/RLI.0000000000001291

calcifications to isolate iodine enhancement and improve lumen assessment.[13,14]

Previous studies have shown that spectral PCD-CT can substantially improve image quality[15] and may enhance the assessment of carotid plaque composition.[16,17] One study demonstrated increased image contrast at lower energy levels,[15] while others showed the potential to segment soft-plaque characteristics such as LRNC and IPH.[16,17] However, no study has systematically and comprehensively evaluated both objective image quality and essential diagnostic measurements, such as degree of stenosis and plaque area, across spectral reconstructions for carotid plaque characterization. The aim of this study was therefore to evaluate image quality and carotid plaque and stenosis assessment using PCD-CT across spectral reconstructions, addressing a critical gap for clinically reliable use of PCD-CT.

METHODS

Study Design

This retrospective study included patients who underwent spectral PCD-CT of the carotid arteries and had carotid atherosclerosis, defined as Plaque-RADS ≥2, in at least 1 carotid artery.[7] The local Medical Ethics Committee waived the need for ethical approval for this study (METC azM/UM; 2023–0290).

Scan Protocol and Image Reconstruction

All scans were acquired on the same PCD-CT system (NAEOTOM Alpha; Siemens Healthineers AG, Forchheim, Germany). Patients were scanned in a supine position following intravenous administration of 40 to 50 mL of iodine-based contrast agent (300 mg/mL, Ultravist; Bayer, Berlin, Germany) at 4 to 6 mL/s. Scans were acquired with 60 × 0.4 mm detector collimation, pitch 0.8, rotation time 0.25 seconds at 140 kVp, IQ level 150. Images were reconstructed with a slice thickness of 0.4 mm, a field of view of 174 mm, and a 512 × 512 pixel matrix, using a Qr40 reconstruction kernel and quantum iterative reconstruction (QIR) level 3. Six spectral reconstructions were generated: 4 ME reconstructions (40, 55, 70, and 85 keV), a PL reconstruction, and a VNC reconstruction (Fig. 1). Energy increments of 15 keV were selected in accordance with prior spectral PCD-CT studies.[15] Radiation dose information [CT dose index ($CTDI_{vol}$ and effective dose)] was collected from Radimetrics (Bayer, Berlin, Germany). The effective dose was calculated using a conversion factor of 0.0059.

The Qr40 kernel, recommended for quantitative spectral evaluations, was used for the primary analysis. Because this kernel is not routinely applied in clinical practice, a separate substudy evaluated lumen and plaque image quality using vascular kernels (Bv40 and Bv56) and varying slice thicknesses (0.2, 0.4, and 1.0 mm). Detailed methods are provided in the Supplementary Methods, Supplemental Digital Content 1, http://links.lww.com/RLI/B111.

Image Analysis

Image analysis was performed by a trained observer using Syngo.via (VB80F, Siemens) and Fiji software.[18] Quantitative evaluation of spectral reconstructions included assessment of technical image quality metrics [signal-to-noise ratio (SNR), contrast-to-noise ratio (CNR), and lumen and calcification edge sharpness], and clinically relevant carotid plaque measurements, including plaque area, degree of stenosis, and attenuation of the lumen and plaque components (IPH, LRNC, fibrous tissue, and calcification). Representative examples of all measurements are shown in Figure 2.

CNR was defined as the difference in attenuation between the carotid lumen and adjacent muscle, with noise quantified as the SD in a homogeneous region of subcutaneous fat (Fig. 2A). SNR was defined as the attenuation of the carotid lumen divided by the noise. Regions of interest (ROIs) were drawn on 5 consecutive slices of the ME 70 keV reconstruction, and the corresponding ROIs were copied to all other reconstructions. Intraobserver reliability for CNR measurements was excellent (ICC = 0.98). Carotid lumen ROIs were drawn on slices with the largest lumen diameter, with a minimal distance from the vessel wall, calcifications, and noncalcified plaque of at least 2 voxels to minimize partial volume effects.

Edge sharpness was determined by extracting slopes from line profiles across perivascular-lumen and lumen-calcification transitions (Fig. 2B). Perivascular-lumen transitions were assessed at the base of the common carotid artery to avoid inclusion of plaque. Slopes were computed using spline interpolation between the 10th and 90th percentiles of the maximum attenuation and normalized to the maximum attenuation to account for energy-dependent attenuation. Δx was the x-axis distance between these 2 points. Sharpness of lumen-calcification transitions was not assessed on PL images, as calcifications are suppressed by the PL algorithm. Edge sharpness was not evaluated on VNC images, since the iodine is virtually eliminated by the VNC algorithm.

Plaque area was defined as the manually delineated vessel wall area on the 5 consecutive slices with the largest plaque burden (Fig. 2C). The degree of stenosis was measured using the NASCET method. Cross-sectional slices of the maximal narrowing and a distal plaque-free segment were reconstructed after manual carotid centerline reconstruction and validated on longitudinal views (Fig. 2D). To assess measurement reliability, plaque area and stenosis measurements were compared with expert consensus, showing excellent interobserver agreement (ICC > 0.89). Plaque area and degree of stenosis could not be assessed on VNC images, as the iodine is removed by the VNC algorithm, and the lumen-plaque interfaces are therefore not discernible.

Plaque component attenuation was analyzed by segmenting the total plaque area ROIs on the ME70 reconstruction based on predefined HU thresholds: IPH: <25 HU, LRNC: 25 to 59 HU, fibrous tissue: 60 to 130 HU, and calcification: >130 HU (Fig. 2C). These plaque component ROIs were then copied to the other reconstructions to assess attenuation values of the same anatomic regions. These thresholds are widely used for carotid plaque segmentation in EID-CT and are incorporated in established classification frameworks.[7,9,19] ROIs were segmented on ME70 as 70 keV corresponds to the mean energy of a typical 120 kVp spectrum in conventional EID-CT.[20] Plaque thresholds derived for conventional 120 kVp images are therefore expected to also apply to ME70 images.[20]

Statistical Analyses

Statistical analyses were conducted using SPSS Statistics version 28 (IBM; Armonk, NY). Normality was evaluated using Shapiro-Wilk tests. Patient characteristics were reported as mean ± SD or as counts with percentages. Differences in all continuous variables (CNR, SNR, noise, sharpness, tissue attenuation, plaque area, and degree of stenosis) across spectral reconstructions were assessed using repeated-measures analysis of variance, followed by Bonferroni-adjusted post hoc pairwise comparisons. Effect sizes of significant pairwise differences were estimated using Cohen *d*. Degrees of stenosis were further

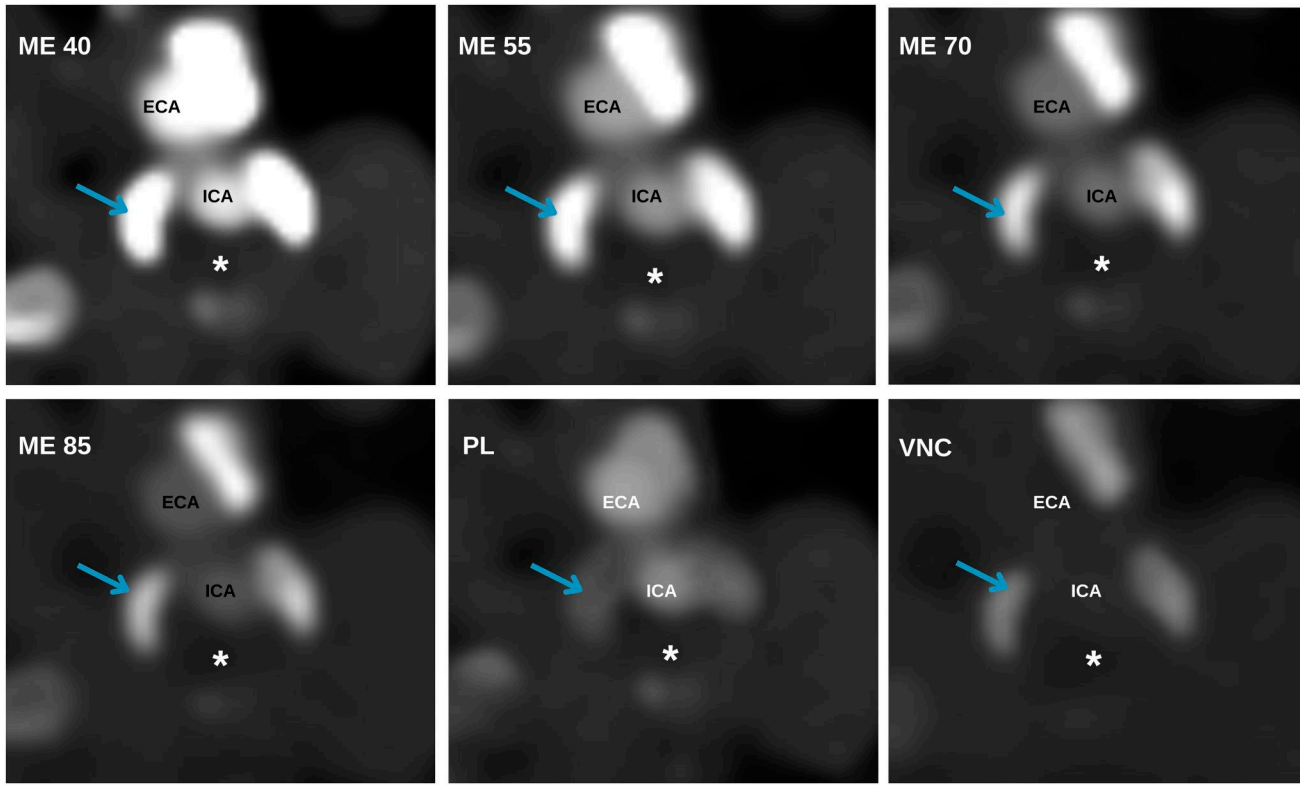

FIGURE 1. Spectral reconstructions of a cross-sectional reconstruction of a carotid plaque from a photon-counting computed tomography scan, displayed at identical window and level settings for objective comparison. The asterisk (*) denotes soft plaque, and the blue arrow indicates a calcification. ECA indicates external carotid artery; ICA, internal carotid artery; ME, monoenergetic; PL, pure lumen; VNC, virtual noncontrast.

categorized into clinically relevant groups ($< 50\%$, 50% to 69%, and $\geq 70\%$). Differences across stenosis categories were assessed using the Friedman test, followed by post hoc pairwise comparisons with the Wilcoxon signed-rank tests. The statistical significance threshold was set at $P < 0.05$.

RESULTS

Patient Characteristics

A total of 27 patients were included, and both carotid arteries were analyzed. Carotid plaques were present in 50 out of 54 arteries (93%). The mean age of the patients was 74.5 ± 9.1 years, and 59% were male. The mean degree of stenosis was $44.5 \pm 28.6\%$, and 28 plaques (52%) were calcified (Table 1). Median $CTDI_{vol}$ was 11.5 (10.9 to 11.7) mGy, and the effective dose was 2.13 ± 0.32 mSv.

Contrast, Signal Intensity, Noise, and Sharpness

As illustrated in Figure 3, lumen-to-muscle CNR, lumen SNR, and image noise decreased progressively with increasing ME levels. The PL reconstruction yielded results comparable to ME55. Due to iodine suppression, VNC reconstructions exhibited CNR and SNR values approaching 0. Pairwise comparisons demonstrated significant differences between reconstructions (Cohen *d*: 0.82 to 2.00, all $P < 0.001$), except between ME55 and PL for both CNR and SNR (both $P = 0.25$), and between ME70 and VNC for noise ($P = 1.00$).

Figure 4 illustrates edge sharpness metrics, normalized slope, and Δx, at the perivascular-lumen and the lumen-calcification transitions. For the perivascular-lumen transition, the normalized slope decreased, and Δx increased with higher ME reconstructions, indicating reduced sharpness at higher keV. PL again performed comparably to ME55. For normalized slope, all reconstructions differed significantly (Cohen *d*: 0.59 to 0.86, all $P < 0.001$), except ME55 versus PL ($P = 1.00$). For Δx, all pairwise differences were significant (Cohen *d*: 0.41 to 0.55, all $P < 0.05$), except ME55 versus ME70 ($P = 0.11$), ME70 versus ME85 ($P = 1.00$), and ME55 versus PL ($P = 1.00$).

At the lumen-calcification edge, normalized slope remained stable across energy levels, with no significant differences between reconstructions (all $P > 0.19$). In contrast, Δx increased slightly with higher energies and differed significantly across reconstructions (Cohen *d*: 0.61 to 1.21, all $P < 0.02$), except ME55 versus ME70 ($P = 0.12$).

Plaque Area and Degree of Stenosis

As shown in Figure 5, mean plaque area did not differ significantly across spectral reconstructions for all plaques, nor when stratified by noncalcified and calcified plaques (all $P > 0.06$), indicating stable plaque area measurements across ME reconstructions and PL. The mean degree of stenosis was highly consistent across all ME reconstructions, ranging from 44 to 45% (all $P = 1.00$), demonstrating strong measurement stability within the ME reconstructions. In contrast, stenosis measured on PL (38%) was significantly lower than on any ME reconstruction (Cohen *d*: 0.61 to 0.65, all $P < 0.001$). Stratification by plaque calcification revealed no significant differences in the degree of stenosis between PL and ME reconstructions in

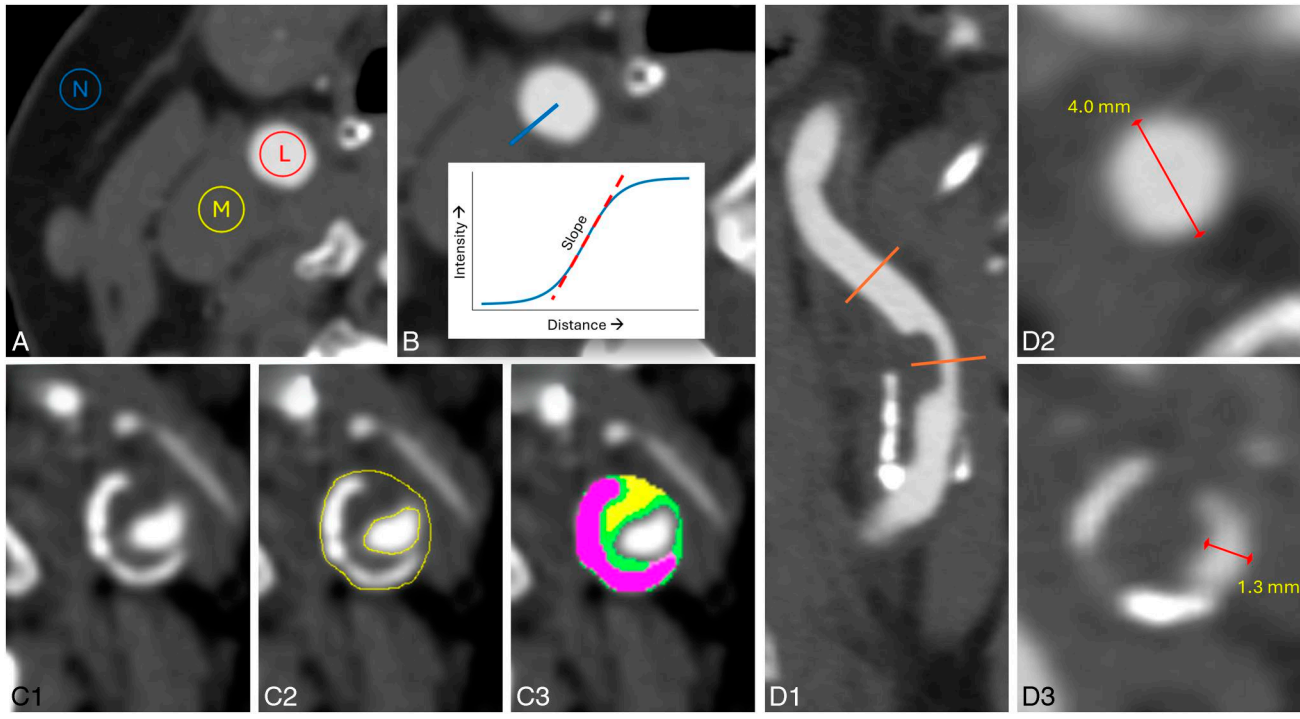

FIGURE 2. Representative examples of quantitative measurements. A, Signal-to-noise ratio (SNR) and contrast-to-noise ratio (CNR) calculated from lumen (L) and muscle (M) attenuation, with noise defined as the SD of the attenuation of subcutaneous fat (N). SNR = mean(L)/SD(N); CNR = (mean(L) − mean(M))/SD(N). B, Edge sharpness is determined from the slope of a line profile across the perivascular-lumen interface. Line placement is indicated by the blue line. C1, Carotid plaque with manually delineated plaque area (C2) and automatic segmentation of plaque components based on HU thresholds: lipid-rich necrotic core (yellow), fibrous tissue (green), and calcification (magenta) (C3). D1, Stenosis measurements according to NASCET criteria. Orange lines indicate a plaque-free distal reference segment (D2) and the segment of maximal narrowing (D3). Diameters are marked with red lines. NASCET stenosis = [(D2 − D3)/D2] × 100%.

noncalcified lesions (all $P = 1.00$), with mean stenosis ranging from 30% to 31% across ME reconstructions and measuring 31% on PL. In calcified lesions, a systematic reduction in measured stenosis was observed on PL: stenosis ranged from 55% to 56% across all ME reconstructions, whereas PL measured an average of 44% (Cohen *d*: 0.97 to 1.08, all $P < 0.001$). Figure 6 presents representative examples of a calcified and a noncalcified stenotic internal carotid artery plaque, illustrating the marked reduction in apparent stenosis on the PL reconstruction observed in calcified plaques, whereas the degree of stenosis in the noncalcified plaque remains unaffected.

Classification of stenosis into clinically relevant groups differed significantly across spectral reconstructions for all plaques and for calcified plaques (both $P < 0.001$), whereas no significant differences were observed for noncalcified plaques (Table 2). Post hoc pairwise analysis indicated that classifications did not differ between ME reconstructions, whereas PL systematically shifted patients in the lower stenosis group categorization compared with all ME reconstructions (all $P < 0.02$). In calcified plaques, the proportion of lesions classified as ≥ 70% stenosis decreased from 32% to 42% across ME reconstructions to a single case (3%) on PL, whereas the proportion classified as nonsignificant (< 50%) stenosis increased from 29% to 39% across ME reconstructions to 52% on PL.

TABLE 1. Patient Characteristics

Per-patient characteristics (n = 27)	
Age, years	74.5 ± 9.1
Sex	
Male	16 (59)
Female	11 (41)
Per-vessel characteristics (n = 54)	
Presence of carotid plaque	50 (93)
Degree of stenosis at 70 keV, %	44.5 ± 28.6
Stenosis severity at 70 keV	
< 50 %	26 (48)
50-69 %	16 (30)
≥ 70 %	12 (22)
Calcified plaque	28 (52)

Data are presented as mean ± SD or n (%).

Lumen and Plaque Component Attenuation

Lower-energy reconstructions resulted in higher attenuation across all tissues and improved separation of plaque components (Fig.7). For PL, lumen attenuation exceeded that of calcification, whereas for VNC, lumen attenuation was markedly reduced and overlapped with fibrotic tissue. Attenuation values differed significantly between all plaque components across reconstructions (Cohen *d*: 1.40 to 4.73, all $P < 0.04$), except for lumen versus calcification at ME40 ($P = 0.11$) and lumen versus fibrous tissue on VNC ($P = 1.00$).

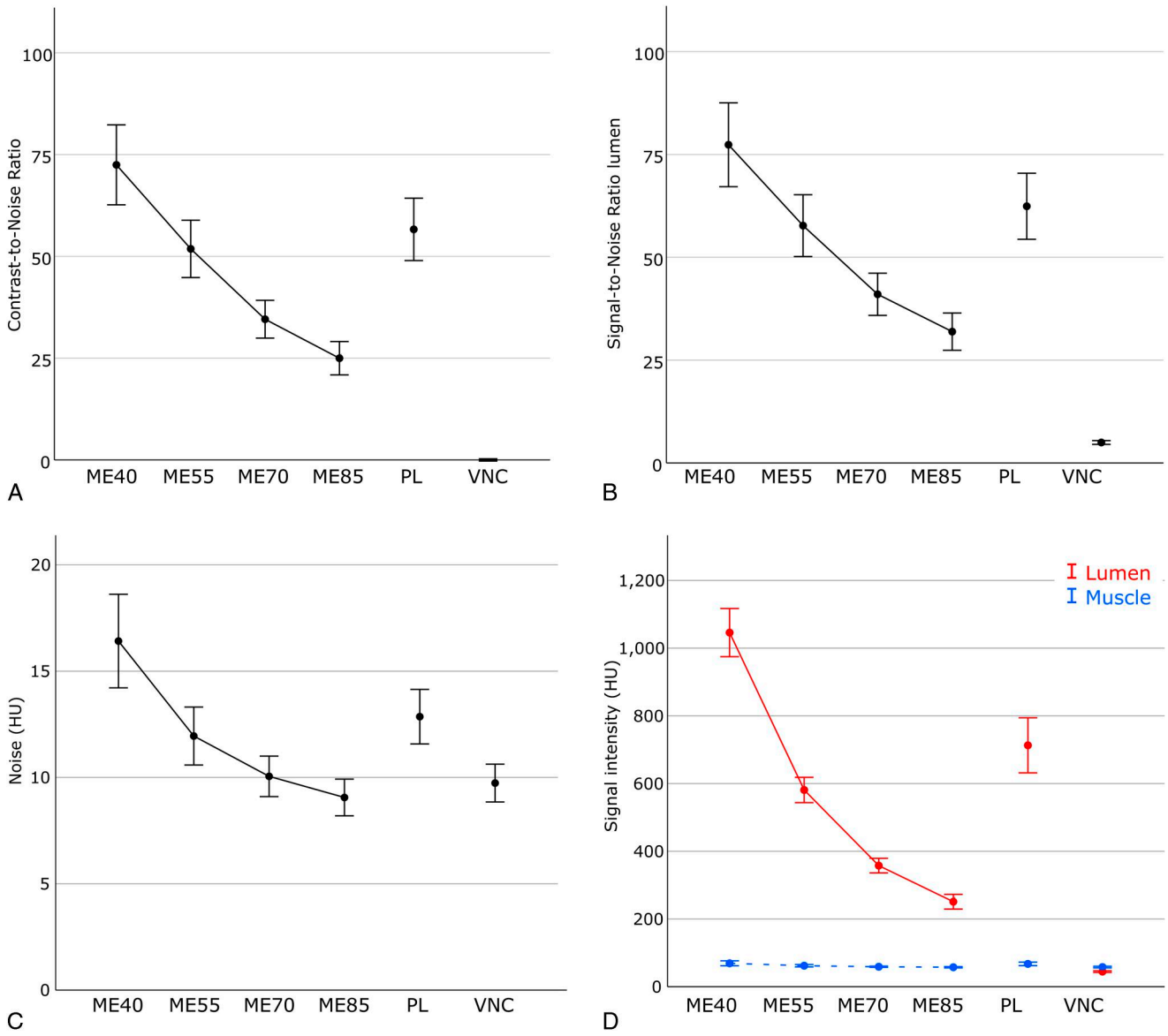

FIGURE 3. Contrast-to-noise ratio (CNR) for lumen-to-muscle contrast (A), lumen signal-to-noise ratio (SNR, B), noise (C), and signal intensity of lumen and muscle (D) with 95% CIs for the different spectral reconstructions. HU indicates Hounsfield unit; ME, monoenergetic; PL, pure lumen; VNC, virtual noncontrast.

Supplementary Analysis

The substudy (Supplementary Results, Supplemental Digital Content 1, http://links.lww.com/RLI/B111) demonstrated that the Bv56 kernel significantly improved subjective lumen image quality (4.8 ± 0.5 vs. 3.7 ± 0.8, $P = 0.008$) compared with Bv40. Slice thicknesses of 0.4 and 0.2 mm reconstructed with a Bv40 kernel performed comparably, both yielding superior image quality relative to 1.0 mm.

DISCUSSION

Our comprehensive evaluation of carotid plaque and stenosis assessment demonstrated that spectral PCD-CT enhances image contrast for carotid plaque assessment, without affecting key diagnostic measurements, namely plaque area and stenosis degree. Lower monoenergetic reconstructions increased lumen-to-muscle contrast, improved edge sharpness, and achieved larger separation of attenuation values between the lumen and plaque components, albeit with higher image noise. Crucially, plaque area and degree of stenosis remained stable across monoenergetic reconstructions, indicating that core diagnostic metrics are robust with substantial gains in image contrast at lower energy reconstructions. By contrast, the PL algorithm matched ME55 in contrast and sharpness but consistently reduced measured stenosis, frequently reclassifying patients to a lower severity. Because carotid stenosis severity directly guides revascularization decisions, the use of PL could substantially lower the number of patients with an indication for intervention.

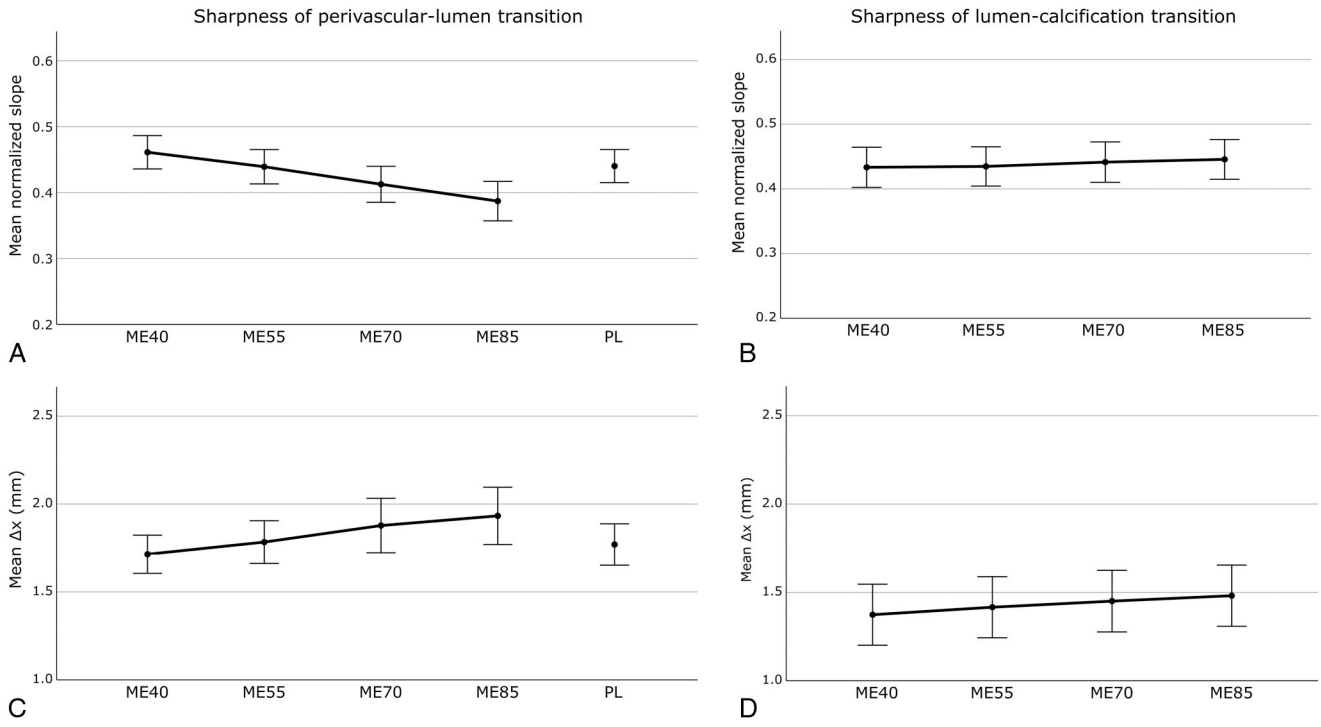

FIGURE 4. Mean normalized slope and mean Δx with 95% CIs for perivascular—lumen transitions (A, C) and lumen-calcification transitions (B, D) across spectral reconstructions. ME indicates monoenergetic; PL, pure lumen.

Contrast, Noise, and Sharpness

We observed increased CNR and SNR of the lumen at lower ME levels, consistent with prior carotid studies.[15] PL performed similarly to ME55, which is expected given that it is derived from the ME55 reconstruction and should approximate it in the absence of calcifications. As anticipated, VNC reconstructions yielded near-zero lumen attenuation, confirming that they mimic noncontrast imaging.[13]

Because lumen and calcification delineation are critical for accurate plaque assessment, we also evaluated edge sharpness using normalized slope and Δx. The normalized slope quantifies the transition rate independent of absolute attenuation, thereby representing intrinsic edge sharpness. We found sharper lumen-perivascular transitions at lower ME reconstructions, with PL again resembling ME55. These findings align with coronary PCD-CT studies that reported sharper luminal edges at lower keV.[21] In contrast, calcification sharpness remained largely unchanged across ME levels, suggesting that blooming observed at lower energies may be related to increased attenuation rather than reduced intrinsic sharpness.

Plaque Area and Stenosis Measurements

Despite the reduction in stenosis grade observed on PL compared with ME reconstructions, plaque area and stenosis degree did not vary across ME reconstructions, reinforcing previous findings from both carotid and coronary studies using spectral CT.[21,22] This is clinically relevant, as the degree of stenosis is still a principal criterion for revascularization in patients with carotid artery disease.[5] Our results indicate that varying keV levels in PCD-CT do not appear to bias stenosis measurements and are therefore unlikely to influence treatment decisions.

A reduction in calcification sharpness at lower ME levels, hypothesized to result from blooming, was not observed. Instead, our data suggest that apparent blooming at lower energies primarily reflects increased attenuation rather than a true loss of sharpness, and that this effect can be visually controlled with optimized window leveling. This is in line with a phantom study that demonstrated energy-dependent blooming could be minimized through appropriate windowing.[23] Although our study lacked phantom data to directly characterize blooming, the stability of stenosis measurements across energies suggests that clinical evaluation is largely robust to this artifact. Future phantom studies should quantify the relationships among attenuation, sharpness, blooming, and stenosis accuracy.

Compared with ME reconstructions, which are conventionally used for stenosis assessment, PL revealed a reduced degree of stenosis, particularly in calcified plaques, consistent with its suppression of calcification signals. This effect was not observed in noncalcified plaques, indicating that PL primarily impacts stenosis quantification when calcification is present. The finding supports the notion that calcifications obscure true lumen size and can cause increased apparent stenosis on CTA.[10] Notably, the lower stenosis measurements on PL frequently led to reclassification into less severe categories. Strikingly, 32% to 42% of calcified plaques were classified as ≥ 70% stenosis on ME reconstructions, whereas only 1 plaque (3%) remained ≥ 70% on PL. These substantial shifts in stenosis classification could profoundly influence clinical decision-making, as current evidence and guidelines for carotid revascularization in symptomatic patients are mainly based on stenosis severity.[5,24] The use of PL instead of ME reconstruction could potentially shift treatment recommendations from a strong indication for revascularization (≥ 70% stenosis) to a recommendation against intervention (< 50% stenosis).[5,24] However, we did not have a

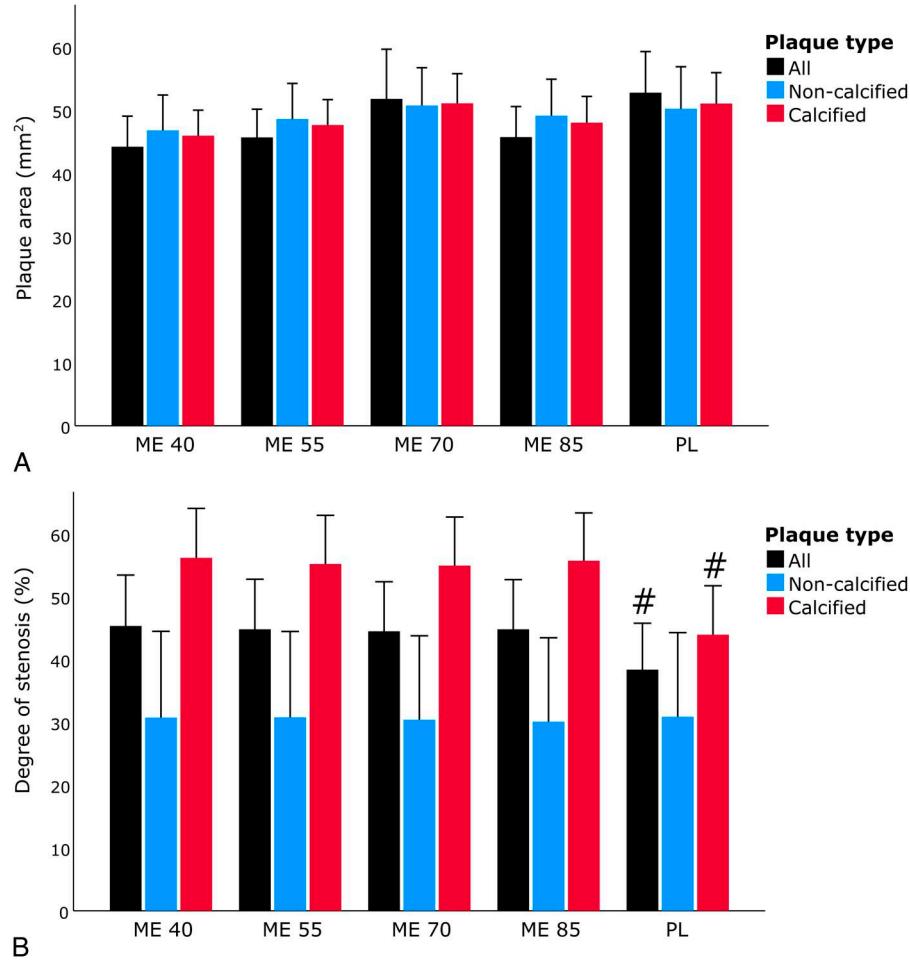

FIGURE 5. Mean plaque area (A) and degree of stenosis (B) across spectral reconstructions, stratified by noncalcified and calcified stenotic lesions. #PL group differs significantly from all ME reconstruction groups (Bonferroni-adjusted post hoc pairwise comparisons).

ground truth stenosis measurement and could therefore not assess whether the decreased degree of stenosis is closer to the actual degree of stenosis. Importantly, a previous coronary phantom study demonstrated that PL-based stenosis assessment reduced overestimation of stenosis compared with monoenergetic reconstructions at the same energy (65 keV), suggesting that PL may provide a more accurate assessment of true stenosis than monoenergetic reconstructions.[14]

The divergent effects of PL on plaque area versus stenosis are attributable to measurement definitions. Plaque area, averaged across multiple slices, is relatively robust to small changes in calcification blooming. In contrast, stenosis grading depends on a single minimal luminal diameter, making it highly sensitive to subtle changes at the lumen-wall interface.

Plaque Composition Assessment

Lower ME reconstructions improved differentiation of the lumen and plaque components, suggesting enhanced capability for compositional assessment. PL and VNC reconstructions altered lumen attenuation in distinct ways: PL reduced calcification attenuation to values below lumen attenuation, whereas VNC reduced lumen attenuation to approximate fibrotic tissue. CT attenuation values are inherently semiquantitative and influenced by reconstruction algorithms, particularly in PL and VNC images. However, all scans were acquired and reconstructed using identical settings, supporting the reliability of relative comparisons across reconstructions. Our HU-based analysis was intended to assess differences between reconstructions rather than absolute tissue characterization. Future studies should evaluate plaque composition assessment using non–HU-based approaches, such as material decomposition, iodine density, or effective atomic number, and validate these against a reference modality.

Our findings add to the growing body of evidence suggesting that spectral PCD-CT has the potential to enhance plaque assessment beyond conventional EID-CT. Prior ex vivo studies have shown encouraging results, including differentiation of IPH and LRNC and quantification of fibrous cap thickness, results that were not achievable with conventional EID-CT.[16,25] More recently, a proof-of-concept in vivo study in 10 patients indicated that clinically indicated PCD-CT could differentiate between IPH, LRNC, and fibrotic tissue against histologic reference.[17]

Improved compositional imaging is clinically relevant, as carotid plaque vulnerability, beyond stenosis, is increasingly recognized as a key determinant of stroke risk.[6,7] While carotid MRI remains the reference standard for soft-plaque characterization, it is less available and less routinely used in clinical settings.[7–9,26]

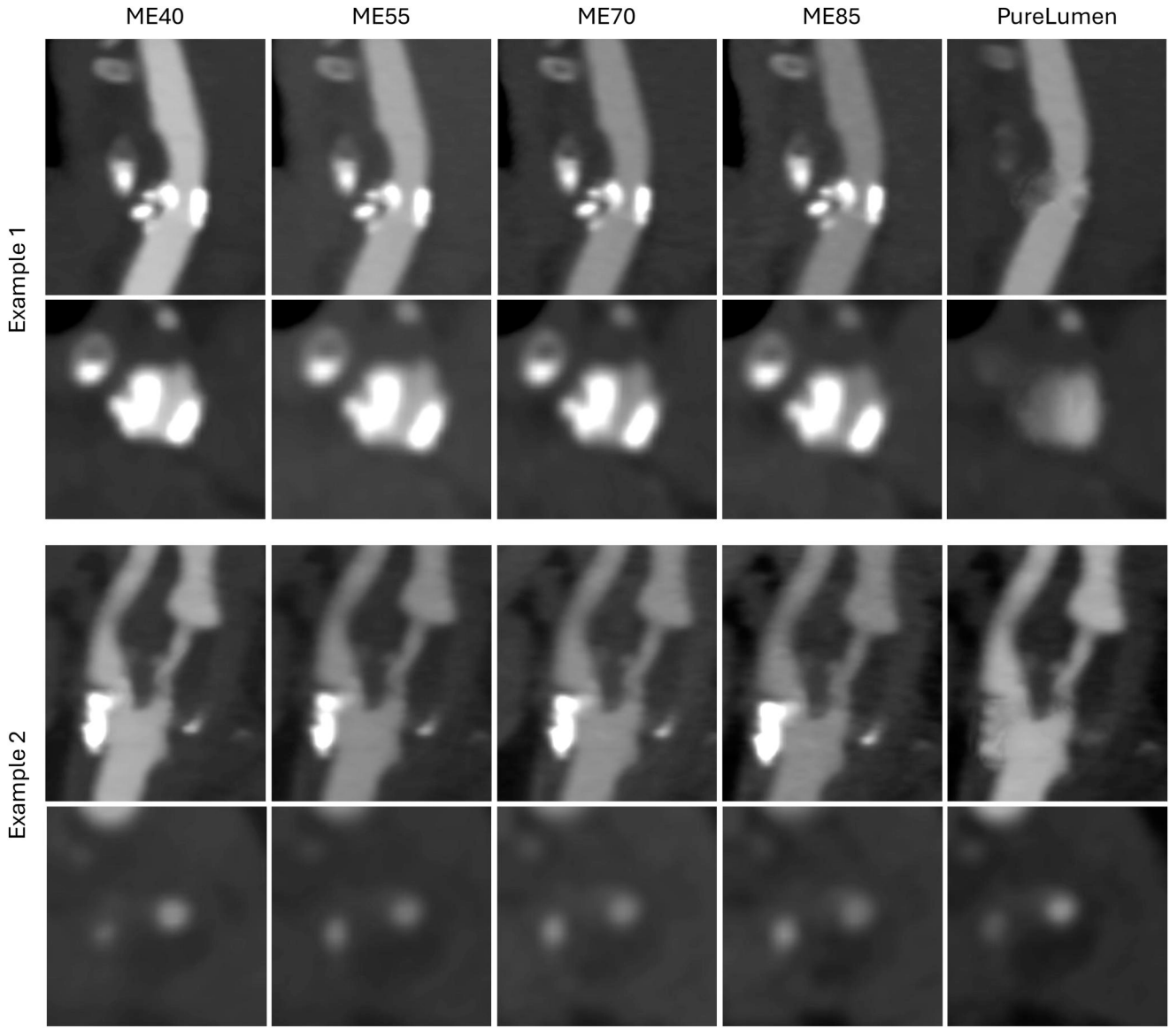

FIGURE 6. Representative monoenergetic (ME) and PureLumen (PL) reconstructions of a calcified internal carotid artery stenotic plaque (example 1) and a noncalcified stenotic internal carotid artery plaque (example 2). In the calcified plaque, the PL reconstruction markedly reduces the apparent degree of luminal stenosis compared with ME reconstructions. In the noncalcified plaque, the apparent degree of stenosis is preserved across PL and ME reconstructions.

Because CTA is already acquired for stenosis assessment, PCD-CT has the potential to integrate plaque characterization into routine workflows, reducing reliance on MRI. If validated against MRI or histology, this could enable clinicians to assess both luminal stenosis and plaque vulnerability with a single CTA examination. Nevertheless, evidence directly comparing PCD-CT with MRI or histology remains limited, and such validation will be essential before soft-plaque assessment with PCD-CT can be adopted for routine clinical decision-making.

Limitations

Our study has several limitations. First, as a retrospective analysis of clinically available PCD-CT scans, no direct comparisons were possible with conventional EID-CT, DSA, MRI, or histology, which limits the assessment of absolute diagnostic accuracy. Nevertheless, we showed that ME reconstructions do not alter key diagnostic measurements for carotid plaque assessment. Although ME70 reconstructions approximate the attenuation of 120 kVp EID-CT scans, the inherently higher spatial resolution of PCD-CT could have influenced our findings. Direct comparison with EID-CT and dual-energy CT was not feasible due to the retrospective design and ethical constraints associated with additional radiation exposure. Moreover, although widely accepted attenuation thresholds were applied for plaque component differentiation, multisequence carotid MRI or histology was not available to confirm the increased separation of plaque components at lower energies. The absence of a ground truth for plaque area and stenosis further precluded evaluation of accuracy, particularly regarding the effect of PL on stenosis grading. Future prospective studies should directly compare

TABLE 2. Degree of Stenosis Measurements Across Spectral Reconstructions Classified Into Clinically Relevant Groups, Stratified by Noncalcified and Calcified Stenotic Lesions

	ME40, n (%)	ME55, n (%)	ME70, n (%)	ME85, n (%)	PL, n (%)	*P**
All						< 0.001†
< 50	24 (48)	23 (46)	22 (44)	21 (42)	28 (56)	
50-69	10 (20)	13 (26)	16 (32)	14 (28)	18 (36)	
≥ 70	16 (32)	14 (28)	12 (24)	15 (30)	4 (8)	
Noncalcified						0.39
< 50	12 (63)	12 (63)	12 (63)	12 (63)	12 (63)	
50-69	4 (21)	5 (26)	5 (26)	5 (26)	4 (21)	
≥ 70	3 (16)	2 (11)	2 (11)	2 (11)	3 (16)	
Calcified						< 0.001†
< 50	12 (39)	11 (35)	10 (32)	9 (29)	16 (52)	
50-69	6 (19)	8 (26)	11 (35)	9 (29)	14 (45)	
≥ 70	13 (42)	12 (39)	10 (32)	13 (42)	1 (3)	

*Friedman test.
†PL group differs significantly from all other ME reconstruction groups (post hoc pairwise Wilcoxon signed-rank tests).

PCD-CT to EID-CT and dual-energy EID-CT to confirm spectral advantages, correlate PCD-CT with MRI or histology to validate plaque characterization, and include calcified artery phantoms with an iodine-enhanced lumen to study blooming effects across energies. Second, the relatively small sample, drawn from a single scanner and center, limits generalizability. Nevertheless, the cohort included a representative population of carotid disease across all stenosis severities, and observer differences across reconstructions were consistent and statistically robust ($P < 0.001$). Future prospective studies should include larger cohorts to enhance generalizability. Third, we only evaluated one PCD-CT from a single vendor. Algorithms such as PureLumen are vendor-specific, and results may not be applicable to other PCD-CT systems. Fourth, the radiation dose in our cohort ($CTDI_{vol}$: 11.5 mGy; effective dose: 2.13 mSv) was higher than that reported for comparable carotid scans acquired with dual-source EID-CT scanners from the same vendor ($CTDI_{vol}$: 8.9 mGy; effective dose: 1.58 mSv).[27] Nevertheless, radiation dose remains within acceptable limits for diagnostic CTA, though future protocol optimization should aim to reduce this. Lastly, because spectral reconstructions are inherently correlated, Bonferroni correction may be overly conservative, potentially underestimating relevant differences, particularly for plaque composition metrics.

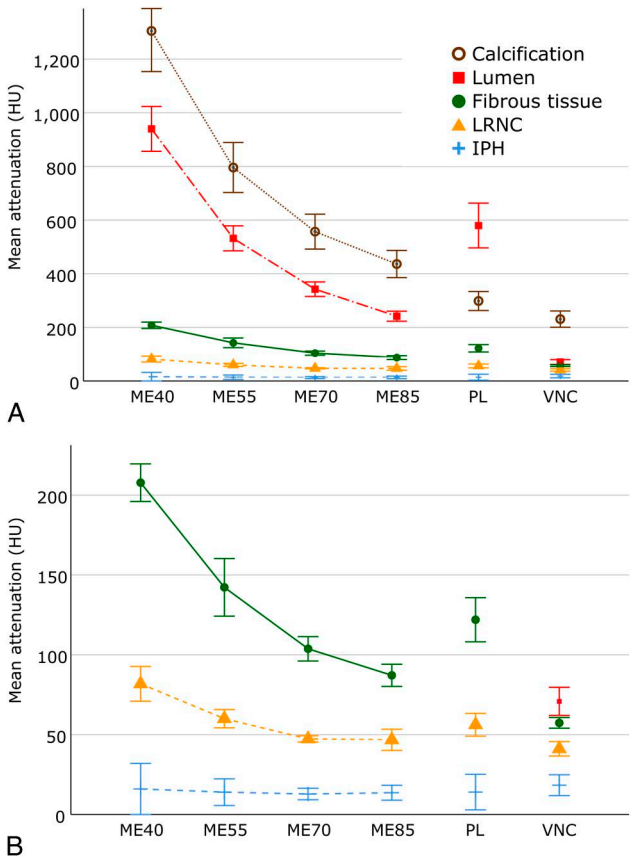

FIGURE 7. A, Mean attenuation with 95% CIs for the lumen and plaque components across spectral reconstructions. B, Zoomed-in view for fibrous tissue, lipid-rich necrotic core (LRNC), and intraplaque hemorrhage (IPH) to highlight differences in attenuation among soft-plaque components. HU indicates Hounsfield unit; ME, monoenergetic; PL, pure lumen; VNC, virtual noncontrast.

CONCLUSION

Low-energy reconstructions with PCD-CT improve contrast and sharpness while maintaining consistent plaque area and stenosis measurements. The degree of stenosis was higher on ME reconstructions compared with the PL algorithm. The PL algorithm may provide additional value in the assessment of the degree of stenosis in calcified plaques, where conventional reconstructions can be affected by artifacts that appear to increase apparent stenosis. Moreover, PCD-CT demonstrates potential for improved plaque composition assessment. Future studies directly comparing PCD-CT with MRI and histology are required to establish its role in soft-plaque assessment.

REFERENCES

1. Cheng SF, Brown MM, Simister RJ, et al. Contemporary prevalence of carotid stenosis in patients presenting with ischaemic stroke. *Br J Surg*. 2019;106:872–878.
2. Kopczak A, Schindler A, Bayer-Karpinska A, et al. Complicated carotid artery plaques as a cause of cryptogenic stroke. *J Am Coll Cardiol*. 2020; 76:2212–2222
3. Saba L, Cau R, Vergallo R, et al. Carotid artery atherosclerosis: mechanisms of instability and clinical implications. *Eur Heart J*. 2025;46:904–921.
4. Gupta A, Baradaran H, Schweitzer AD, et al. Carotid plaque MRI and stroke risk: a systematic review and meta-analysis. *Stroke*. 2013;44: 3071–3077.

5. Bierens J, Speetjens I, van Oostenbrugge RJ, et al. Systematic review of the discrepancies between guideline recommendations on carotid revascularization in patients with symptomatic carotid artery disease. *Stroke Vasc Interv Neurol*. 2025;5:6.
6. Saba L, Brinjikji W, Spence JD, et al. Roadmap consensus on carotid artery plaque imaging and impact on therapy strategies and guidelines: an international, multispecialty, expert review and position statement. *AJNR Am J Neuroradiol*. 2021;42:1566–1575.
7. Saba L, Cau R, Murgia A, et al. Carotid plaque-RADS: a novel stroke risk classification system. *JACC Cardiovasc Imaging*. 2024;17:62–75
8. Bierens J, Postma AA, Frehe K, et al. Comparison of MRI- and CTA-based plaque-RADS to predict stroke and TIA in symptomatic carotid disease. *JACC Cardiovasc Imaging*. 2025. doi:10.1016/j.jcmg.2025.10.009
9. Aizaz M, Bierens J, Gijbels MJJ, et al. Differentiation of atherosclerotic carotid plaque components with dual-energy computed tomography. *Invest Radiol*. 2025;60:508–516
10. Ghouri MA, Gupta N, Bhat AP, et al. CT and MR imaging of the upper extremity vasculature: pearls, pitfalls, and challenges. *Cardiovasc Diagn Ther*. 2019;9(suppl 1):S152–S173.
11. Flohr T, Schmidt B. Technical basics and clinical benefits of photon-counting CT. *Invest Radiol*. 2023;58:441–450.
12. Meloni A, Cau R, Saba L, et al. Photon-counting computed tomography angiography of carotid arteries: a topical narrative review with case examples. *Diagnostics (Basel)*. 2024;14:18.
13. van der Bie J, van Straten M, Booij R, et al. Photon-counting CT: review of initial clinical results. *Eur J Radiol*. 2023;163:110829.
14. Allmendinger T, Nowak T, Flohr T, et al. Photon-counting detector CT-based vascular calcium removal algorithm: assessment using a cardiac motion phantom. *Invest Radiol*. 2022;57:399–405.
15. Booz C, Bucolo GM, D'Angelo T, et al. Carotid artery assessment in dual-source photon-counting CT: impact of low-energy virtual monoenergetic imaging on image quality, vascular contrast and diagnostic assessability. *Radiol Med*. 2024;129:1633–1643.
16. Dahal S, Raja AY, Searle E, et al. Components of carotid atherosclerotic plaque in spectral photon-counting CT with histopathologic comparison. *Eur Radiol*. 2023;33:1612–1619.
17. Shami A, Sun J, Celander M, et al. Clinical photon-counting computed tomography in living patients detects intra-plaque haemorrhage and thrombus in carotid plaques. *Eur Heart J*. 2025;46:5045–5048.
18. Schindelin J, Arganda-Carreras I, Frise E, et al. Fiji: an open-source platform for biological-image analysis. *Nat Methods*. 2012;9:676–682.
19. Saba L, Micheletti G, Brinjikji W, et al. Carotid intraplaque-hemorrhage volume and its association with cerebrovascular events. *AJNR Am J Neuroradiol*. 2019;40:1731–1737.
20. Rassouli N, Chalian H, Rajiah P, et al. Assessment of 70-keV virtual monoenergetic spectral images in abdominal CT imaging: a comparison study to conventional polychromatic 120-kVp images. *Abdom Radiol (NY)*. 2017;42:2579–2586.
21. Sartoretti T, McDermott M, Mergen V, et al. Photon-counting detector coronary CT angiography: impact of virtual monoenergetic imaging and iterative reconstruction on image quality. *Br J Radiol*. 2023;96:20220466.
22. Bai X, Gao P, Zhang D, et al. Plaque burden assessment and attenuation measurement of carotid atherosclerotic plaque using virtual monoenergetic images in comparison to conventional polyenergetic images from dual-layer spectral detector CT. *Eur J Radiol*. 2020;132:109302.
23. McDermott MC, Sartoretti T, Stammen L, et al. Countering calcium blooming with personalized contrast media injection protocols: the 1-2-3 rule for photon-counting detector CCTA. *Invest Radiol*. 2024;59:684–690.
24. Naylor R, Rantner B, Ancetti S, et al. Editor's Choice—European Society for Vascular Surgery (ESVS) 2023 clinical practice guidelines on the management of atherosclerotic carotid and vertebral artery disease. *Eur J Vasc Endovasc Surg*. 2023;65:7–111.
25. Shami A, Sun J, Gialeli C, et al. Atherosclerotic plaque features relevant to rupture-risk detected by clinical photon-counting CT ex vivo: a proof-of-concept study. *Eur Radiol Exp*. 2024;8:14.
26. Bierens J, Ament SMC, Truijman MTB, et al. Plaque magnetic resonance imaging based decision rule for the selection of symptomatic patients for carotid revascularisation: clinician perspectives on acceptability and implementation barriers in the Netherlands. *Eur J Vasc Endovasc Surg*. 2026;71:5–11.
27. Saba L, di Martino M, Siotto P, et al. Radiation dose and image quality of computed tomography of the supra-aortic arteries: a comparison between single-source and dual-source CT scanners. *J Neuroradiol*. 2018;45:136–141.